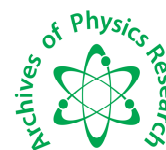




Scholars Research Library

Archives of Physics Research, 2012, 3 (2):106-115
(<http://scholarsresearchlibrary.com/archive.html>)



Scholars Research
Library

ISSN : 0976-0970

CODEN (USA): APRRC7

Structural and dielectric properties of $\text{Sr}_x\text{Ba}_{1-x}\text{Nb}_2\text{O}_6$ ferroelectric ceramics

S. N. Mathad¹ and Vijaya Puri^{*2}

¹Department of Engineering Physics, KLE Institute of Technology, Hubli., India

²Thick and Thin Film Device Laboratory, Department of Physics, Shivaji University, Kolhapur, India

ABSTRACT

This paper reports, the structural, dielectric and transport properties of $\text{Sr}_x\text{Ba}_{1-x}\text{Nb}_2\text{O}_6$ [SBN] for $x = 0.4$ and 0.5 , prepared by traditional sintering method (solid state reaction technique). The tetragonal tungsten bronze type crystal structure, structural parameters such as the lattice constant ($a = 12.63946\text{\AA}$, $b = 12.63946\text{\AA}$, $c = 3.978203462\text{\AA}$), average crystallite size ($61.62\text{ nm}-95.17\text{ nm}$), and texture coefficient (TC) have been determined using X-ray diffraction data. TGA-DTA analysis reveals that formation of oxide phase takes place beyond 1050°C . Rod shaped surface morphology has been obtained. The fundamental vibrational mode observed in finger print region by FTIR reveals formation of SBN ceramics. The variation of real of part dielectric constant (ϵ') and loss tangent ($\tan\delta$) was studied at room temperature. The dispersion of dielectric constant with frequency indicates relaxor nature of SBN.

Key words: .Strontium Barium Niobate, Structural properties, Dielectric Constant, Transport properties.

INTRODUCTION

Ferroelectric materials are an important class of materials whose main characteristic is the presence of a spontaneous polarization that can be changed with an external electric field. In recent years, lead-free ferroelectrics have drawn great attention due to worldwide concern over the toxicity of lead-containing materials. Many studies have been conducted with the aim of finding lead-free compositions competitive to their lead-based counterparts. In view of environmental concerns, lead free materials are being considered for many applications and strontium barium niobates ($\text{Sr}_x\text{Ba}_{1-x}\text{Nb}_2\text{O}_6$) is among the few materials that are in the forefront due to excellent novel technological application properties. The $\text{Sr}_x\text{Ba}_{1-x}\text{Nb}_2\text{O}_6$ (SBN) is an interesting and valuable crystal host for luminescent lanthanide ions [1] pyroelectric, piezoelectric and photorefractive devices [2-3]. These materials are attractive for volume holographic information storage [4], ferroelectric non-linear crystal showing a large number of applications such as data storage, switching, optical computing and more recently as a tunable laser host [5-7].

These SBN ceramics can be synthesized easily but with larger grain size and complex shape application [8-9]. The objective of this work is the synthesis of SBN ferroelectric material by low cost solid state reaction route at low temperature. A detailed significant investigation of the microstructural, vibrational, and dielectric properties are presented and discussed in this paper.

MATERIALS AND METHODS

The high purity AR grade SrCO_3 (99.95%), BaCO_3 (99.95%) and Nb_2O_5 (99.999%) were used as starting materials. Powder was ground for homogenization using agate mortar in acetone medium for 1 hour. This powder was mixed in stoichiometric proportion and ground for 4 hours in acetone medium to obtain desired stoichiometry in the resultant compounds. This mixture was initially sintered at 1200°C for 10 hrs and further at 850°C for 48 hours in a muffle furnace. The flow chart of material preparation is shown in figure 1. The available reports on this material are at higher temperature [10-11].

The following stoichiometric samples were studied $\text{Sr}_{0.4}\text{Ba}_{0.6}\text{Nb}_2\text{O}_6$ (SBN40), $\text{Sr}_{0.5}\text{Ba}_{0.5}\text{Nb}_2\text{O}_6$ (SBN50).

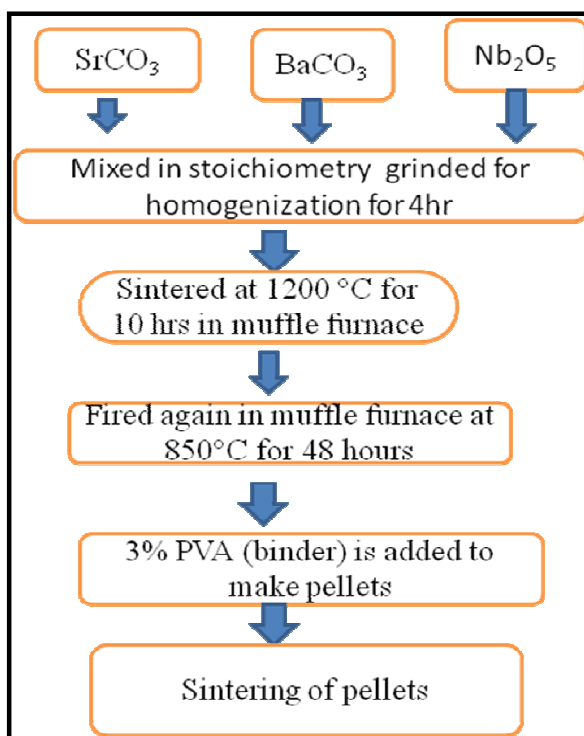


Fig.1 : Flowchart of material preparation

The tetragonal tungsten bronze phase was confirmed by x-ray diffraction using Cr-K_α radiations, (Philips Diffract meter PW 3710). The TGA-DTA measurements were carried out in the range 25 to 1200°C in air, at the rate of 10°C per min on SDT-2960 TA instrument USA. FTIR spectra of powders were recorded by using Perkin-Elmer's Spectrum one Spectrometer in the range of 400 – 4000 cm^{-1} with KBr solvent. This powder was pressed into pellets in a hydraulic press at 10 ton/cm^2 for 5 min. The surface morphology was studied using scanning electron microscope (SEM JEOL-JSM 6360). The frequency dependence permittivity (ϵ') and dissipation factor ($\tan \delta$) in the range from 20 Hz to 1 MHz were studied using a precision LCR meter bridge (model HP 4284 A).

RESULTS AND DISCUSSION

1.TG-DTA analysis

Prior to solid state reaction, we have carried out TG-DTA analysis of precursors mixed in stoichiometric proportion from room temperature to 1200°C , so as to understand the decomposition behavior of the precursors. The thermogram for the same is shown in Figure 2. The plot shows the three major regions. In the first region (27°C - 250°C), the weight loss may be mainly due to the vaporization of water of crystallization and decomposition, i.e. initial weight loss of 2.365% occurred up to temperature around 250°C , accompanied with exothermic reaction. This is due to removal of absorbed water molecule present in precursors. In the second region (300°C to 800°C) sharp

weight loss of 11.5% might be due to the decomposition from 300^o C to 800^o C, which is due to evolution of CO₂ from carbonate precursors. Further increase in temperature no major observed weight loss was observed above 1100 °C indicating the formation of ceramic. Thus the modified formation mechanics of SBN as reported [12]

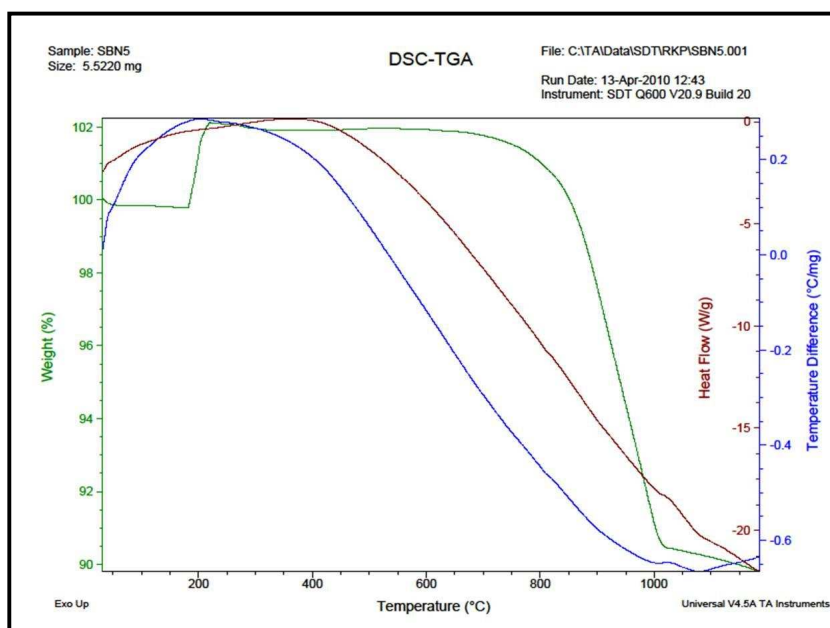
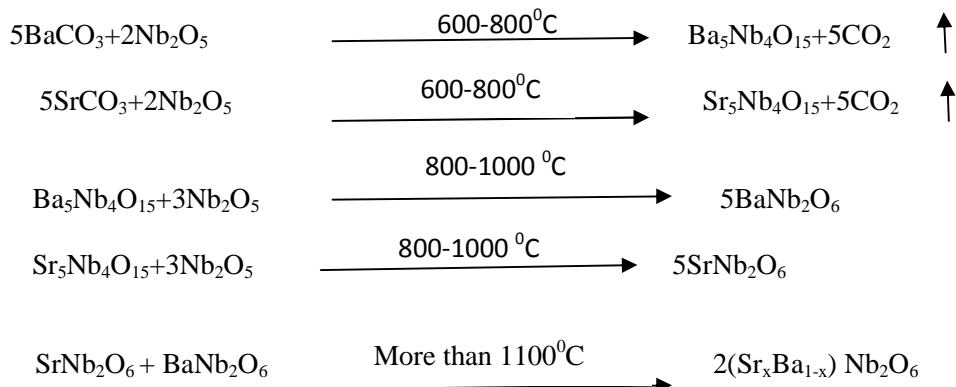


Fig .2 TGA –DTA Graph of SBN50

2. X-ray diffraction analysis:

X-ray diffraction patterns of $\text{Sr}_x\text{Ba}_{1-x}\text{Nb}_2\text{O}_6$ ($x = 0.4, 0.5$) for different compositions are shown in figure 3. From the figure, the formation of pure perovskite tetragonal phase of $\text{Sr}_x\text{Ba}_{1-x}\text{Nb}_2\text{O}_6$ (JCPDS card no 00-039-0265) is confirmed. The calculated lattice parameters for all samples ($a = 12.63946\text{Å}$, $b = 12.63946\text{Å}$, $c = 3.978203462\text{Å}$) were found to be in good agreement with earlier reported values [10-12]. The crystallite size was determined from the Debye-Scherrer equation,[13]

$$D = 0.9\lambda / (\beta \cos \theta)$$

Where D is the diameter of the crystallites of powder, λ is the wavelength of the Cr-K α line, β is the FWHM in radians and θ is Bragg's angle.

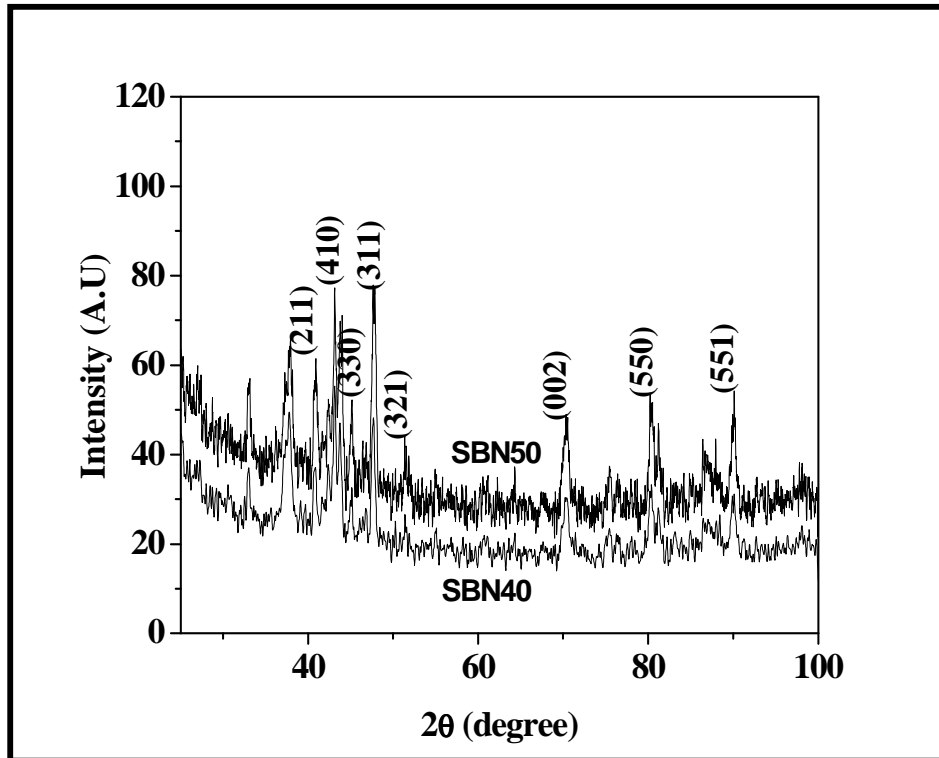


Fig.3. X ray diffractogram of $\text{Sr}_x\text{Ba}_{1-x}\text{Nb}_2\text{O}_6$ with $x=0.40, 0.50$

The lattice constants and crystallite size decreases with increase in strontium content from 95.17nm to 61.62 nm. This is due to the smaller ionic radii of Sr^{+2} (1.54Å) as compared to Ba^{+2} (1.74 Å) [12]. It may be due partial replacement of Ba^{+2} with Sr^{+2} causing the shrinkage of the unit cell dimensions resulting in decrease in the lattice parameter. Quantitative information concerning the preferential crystallite orientation is obtained from texture coefficient. TCs (hkl) defined by relation [13],

Where $I(hkl)$ is the measured intensity, $I_0(hkl)$ is the ASTM intensity and N the reflection number. The calculated texture coefficient (TC) of each plane (hkl) is tabulated in Table 1, the orientation of planes at (002) is more in SBN40 and at (551) in SBN 50 this reorientation effects occurs due to doping.

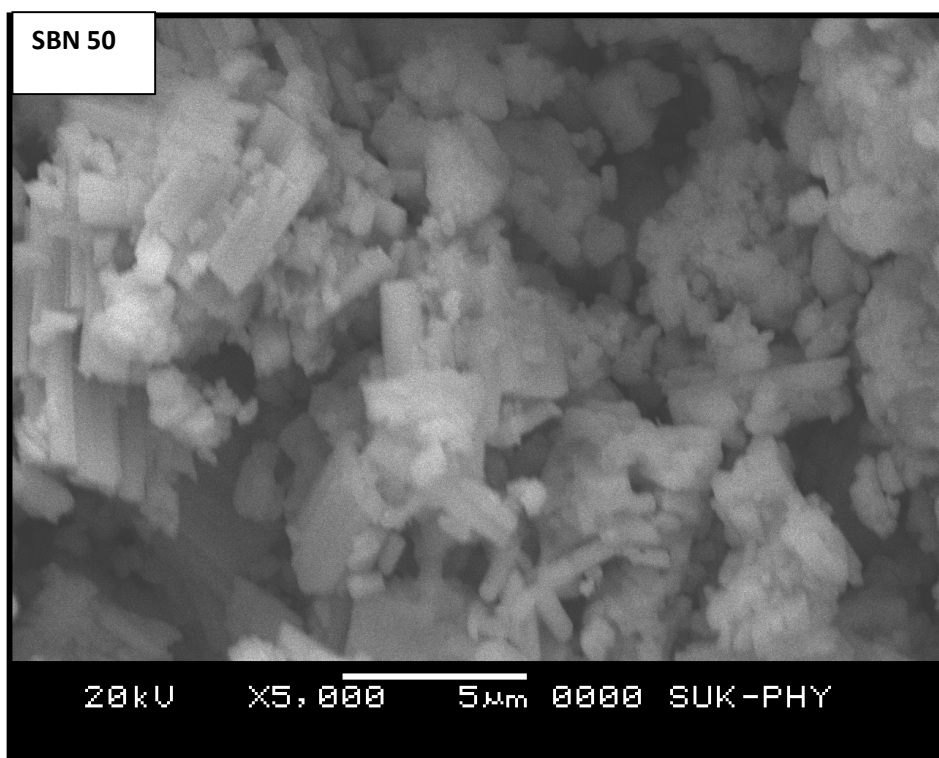
$$TC(hkl) = \frac{\frac{I(hkl)}{I_0(hkl)}}{\frac{1}{N} \sum_N \frac{I(hkl)}{I_0(hkl)}}$$

Table 1: Texture Coefficient of SBN 40 and SBN50

(hkl)	Texture Coefficient TC(hkl)							
	(211)	(410)	(330)	(311)	(321)	(002)	(550)	(551)
SBN 50	0.584615	0.93721	0.932001	0.858841	0.641871	1.423222	1.038598	1.582721
SBN40	0.705025	0.62512	1.137624	0.819964	1.292522	1.48882	0.80242	1.128504

3. Surface morphology:

The SEM micrographs of SBN50 sample are as shown in figure 4..

**Fig.4 SEM image of SBN 50**

These microstructures show different shaped rod structure of length of 1µm to 5µm and width 0.6µm. The porous spaces observed are of much advantageous for sensing applications. These materials can absorb moisture or water into the porous spaces and are potential materials for microwave sensors and other related applications.

4. FTIR study:

Ferroelectric SBN crystals have a tetragonal tungsten bronze structure with space group $P4bm$ (C_{4v}^2). For the $P4bm$ space group there are 138 possible vibrational normal modes and they can be classified according to the following irreducible representations due to complex crystal structure of the material [14]

$$\Gamma^{\text{total}} = 19A_1(z) + 15A_2 + 14B_1 + 18B_2 + 36E(x) + 36E(y)$$

Where x, y, and z indicate the polarization direction of the infrared active modes (z is the ferroelectric axis). Three modes belonging to the A_1 , $E(x)$, and $E(y)$ representations are acoustic modes and the other modes, except A_2 modes, are Raman active; the number of such modes is 120. As we know general formula of a lattice cell of SBN can be written as $(A_1)_4(A_2)_2(B_1)_2(B_2)_8O_{30}$ which has different types of cationic sites are available in this host crystal. The A_1 sites are partially occupied by Sr^{2+} ions, the A_2 sites are randomly occupied by the Sr^{2+} and Ba^{2+} lattice ions, while the B_1 and B_2 sites are completely filled by Nb^{5+} ions and in addition to this cationic disorder, there is also a certain disorder on the O^{2-} anion sublattice [15]. According to SBN crystals the quantum-chemical calculations

(DFT) for the NbO_6^{7-} anion and first approximation, the dynamics of isolated NbO_6^{7-} anions have been taken into account. The calculated vibrational frequencies for the free NbO_6^{7-} ion are in fair agreement with the frequencies of modes observed in experiment as reported elsewhere [14-15].

At room temperature absorption spectra (FTIR) of SBN40 and SBN 50 remains same for both samples as shown in Fig (5). We observe a broad peak in the region 400 to 850cm^{-1} . These peaks are due to superposition of fundamental modes T_{2u} (triple degenerate bending mode) and A_{1g} (symmetric stretching mode) with assignments $\delta(\text{O-Nb-O})$ and $\nu(\text{Nb-O})$ respectively. At region 1600 to 1800cm^{-1} and at 2800 to 3000cm^{-1} we find that bands due to sum of the fundamental modes of T_{2u} and A_{1g} . However, it is observed that IR spectra at about 400 - 800cm^{-1} SBN50 shows dominantly stronger peak than SBN40, these results match the reported ones. [15-16]

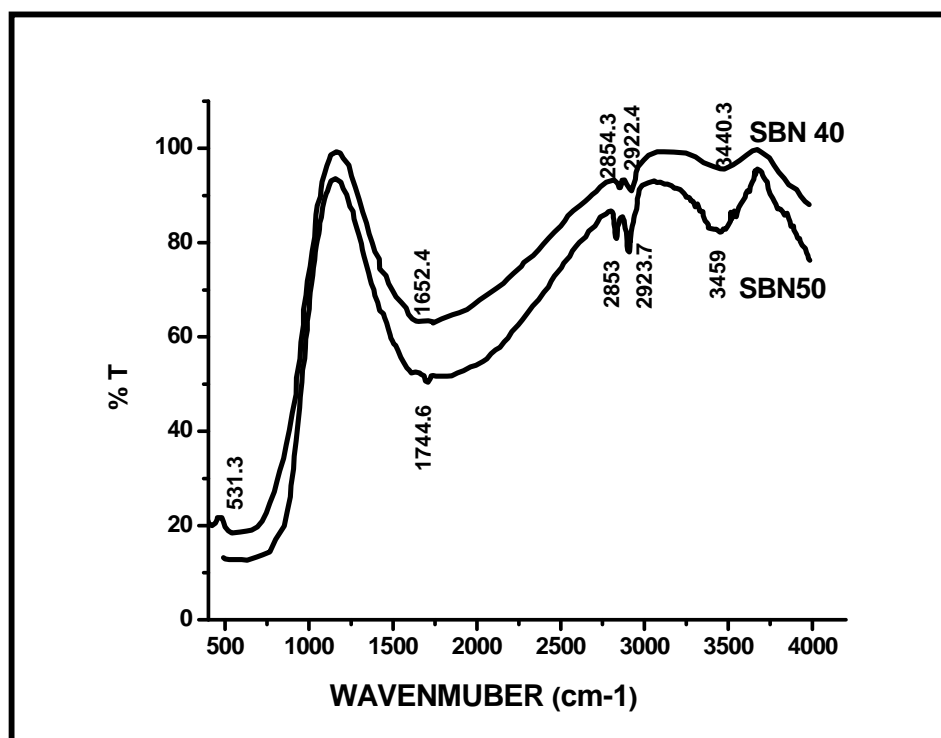


Fig .5.Absorption spectra (FTIR) of SBN40 and SBN 50

As stated before the ionic radii of Sr^{+2} (1.54\AA) is smaller as compared to Ba^{+2} (1.74\AA). Due to increase in concentration of Sr^{+2} in $\text{Sr}_x\text{Ba}_{1-x}\text{Nb}_2\text{O}_6$ the average ionic radius of NbO_6^{7-} environment decreases. There may be stronger deformation of niobate octahedra for higher strontium values. We have also observed SBN crystals studied so far contained only a small amount of hydroxyl ions (OH^-), probably as a result of the humid atmosphere during the growth process.

5. Dielectric permittivity and ac conductivity

The dielectric permittivity (ϵ') of the sample was calculated using the relation

$$\epsilon' = \frac{Cd}{\epsilon_0 A}$$

Where 'C' is the measured value of capacitance of the sample, 'd' is the thickness, 'A' is the surface area, and ' ϵ_0 ' is the dielectric permittivity of free space.

The frequency dependence of the dielectric permittivity (ϵ') for all the samples was studied at room temperature. Figure (6) reveals the variation of dielectric permittivity with frequency from 20Hz to 1MHz . Dielectric permittivity

decreases as frequency increases from 20 Hz to 1 MHz showing usual dielectric dispersion behavior. The decrease in permittivity with frequency can be explained on the basis of Koops theory.

In general, the decreases in permittivities are rapid at lower frequencies and slower at higher frequencies. Similar results were observed for other systems of ferroelectrics, the low frequency dispersion in SBN is observed due to space charge effect and slowly all polarization vanishes at higher frequency except electronic polarisation. When the frequency increases, the number of mechanisms involved in the dynamic polarization decreases. At very high frequencies, only the electronic contribution of the polarization remains. [17-18]

The dielectric structure is assumed to be consisting of well-conducting grains which are separated by poorly conducting grain boundaries. At lower frequencies the grain boundaries are more effective for conductivity and permittivity than grains. Therefore permittivity (ϵ') is high at lower frequencies and decreases as frequency increases. Since it is observed that in dielectrics the the permittivity (ϵ') is directly proportional to the square root of conductivity (σ) [19]. Hence the permittivity (ϵ') high at lower frequencies and decreases as frequency increases, decrease in permittivity is due to jumping frequency of electric charge carriers can not follow the alternation of the applied ac field beyond a certain critical frequency.

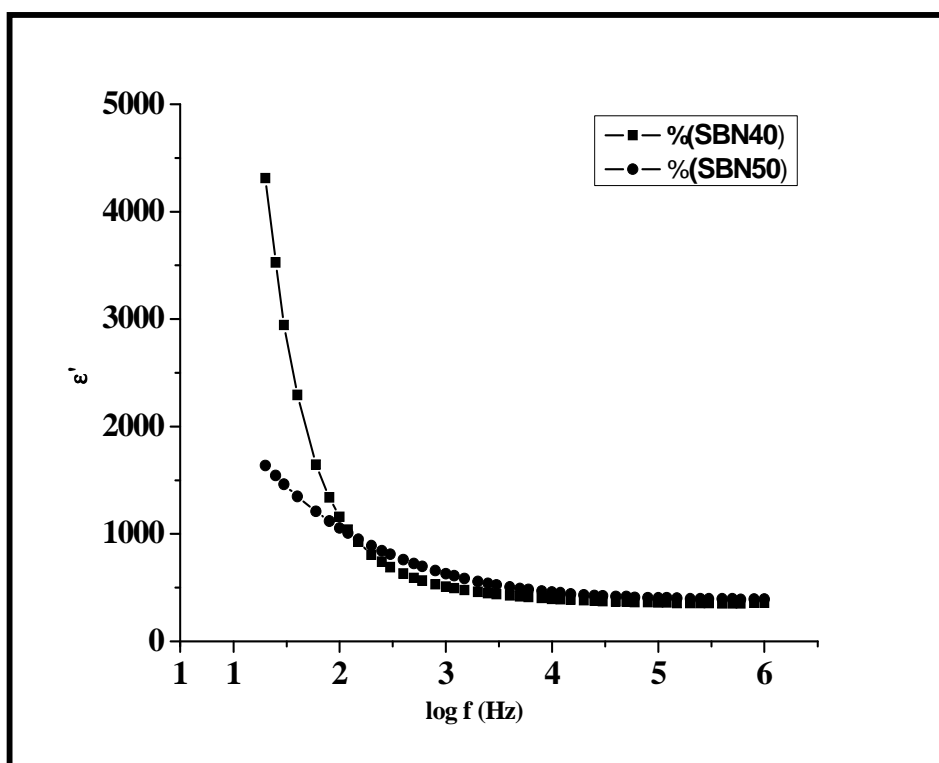


Fig.6. Frequency dependence of the dielectric permittivity (ϵ') of SBN40 and SBN 50

High frequency studies in SBN ceramics the effect of the hopping of off-centred ferroelectric ions has also been proposed by several authors. The tetragonal tungsten bronze phase ceramics (SBN) exhibits at high frequency relaxation in the paraelectric phase and its origin was ascribed to the crystalline network owing to the motion of active ferroelectric Nb^{5+} ions. It is observed that at lower frequency, the dielectric constant of SBN 40 shows higher values than that of SBN 50. In tungsten bronze type relaxor ferroelectrics, the complexity of the structure makes interpretations more difficult. Disorder usually may take place in A_1 and A_2 sites. i.e. its origin is probably related to the relaxor behavior of this material resulting from the cationic disorder of Sr^{+2} and Ba^{+2} in A_1 and A_2 sites. The relaxation phenomena depend on the strontium content. The dispersion is more pronounced in Sr-rich compositions [20-21].

The variation of dielectric loss tangent ($\tan\delta$) with frequency is shown in Fig (7). The loss tangent decreases continuously with increase in frequency and attains a constant value at higher frequencies.

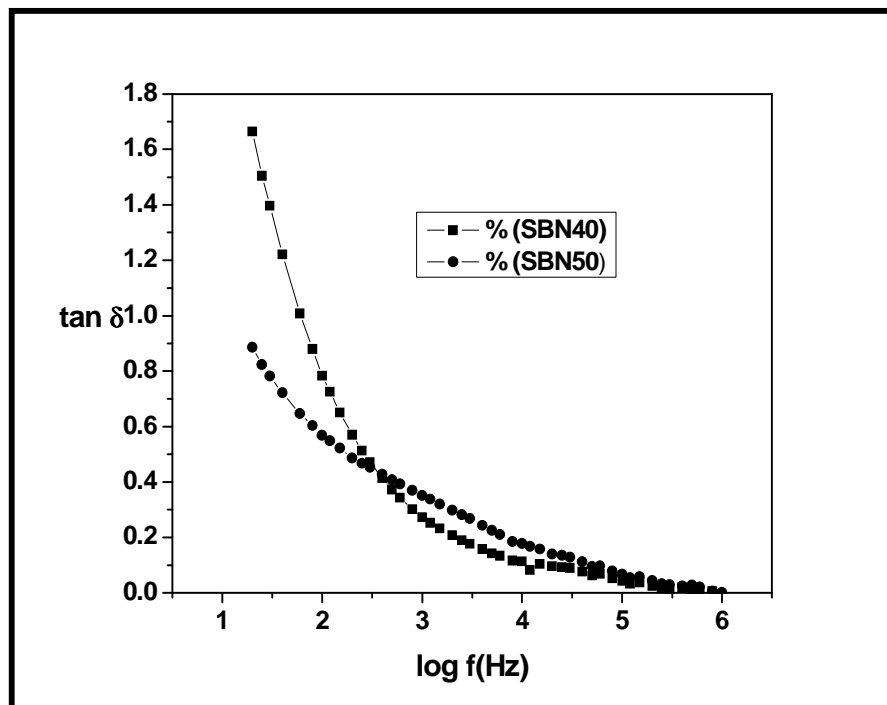
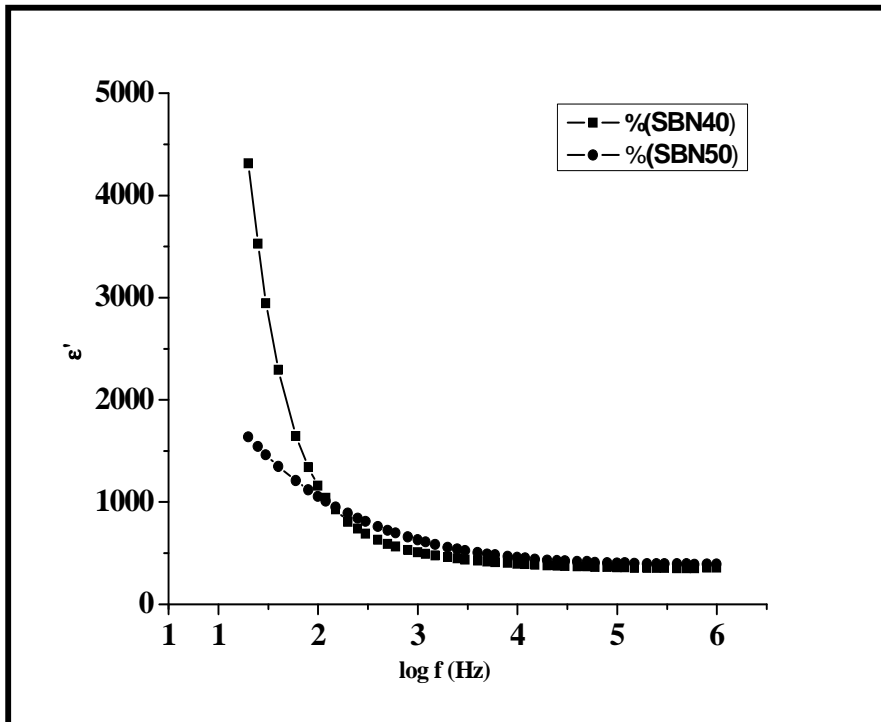


Fig .7.Variation of dielectric loss tangent ($\tan\delta$) with frequency of SBN40 AND SBN50

To understand the conduction mechanism and the type of polarons responsible for conduction, the variation of AC conductivity carried out at room temperature as a function of frequency is represented Fig (8). AC conductivity of samples can be evaluated using the relation

$$\sigma = 2\pi\epsilon_0\epsilon' f \tan \delta$$

where f is the frequency of the applied field, ϵ_0 is the permittivity of free space, ϵ' is the real part of relative permittivity of the samples, $\tan \delta$ is the loss factor and σ ac conductivity.

In large polaron hopping the ac conductivity decreases with frequency and in small polaron hopping conductivity increases with frequency. From graph the conductivity is observed to increase with increase in frequency for all the samples.

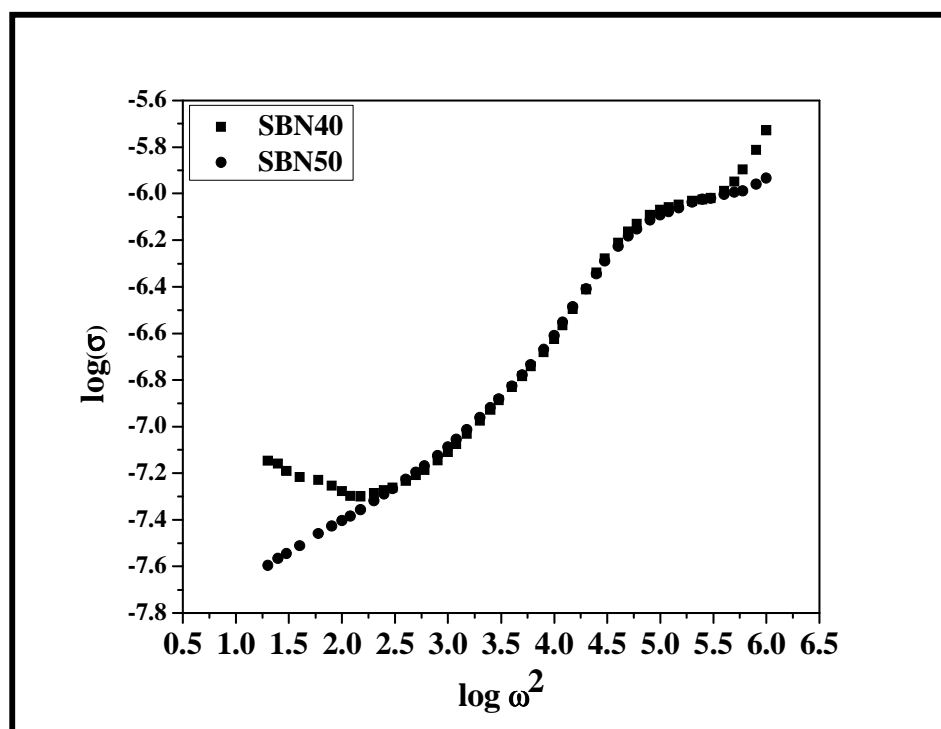


Fig .8. Variation of AC conductivity carried out at room temperature as a function of frequency of SBN40 and SBN50

Due to hopping of charge carriers between localized states the linear variation of ac conductivity observed. On the basis of theoretical models it can be interpreted as indicating that the ac conductivity originates from a migration of ions by hopping between neighboring potential wells. In ionic solids, the electrical conduction is due to migration of ions and this ionic transport depends on the angular frequency. Thus, ac conductivity is proportional to angular frequency confirming linear nature, which eventually gives rise to dc conductivity at the lowest frequencies. [22]

CONCLUSION

The solid state reaction method is useful for the preparation of SBN. The tungsten bronze crystal structure was confirmed from X-ray studies. Rod shaped surface morphology was obtained. Typical absorption peaks at 800 to 450 cm^{-1} in FTIR spectrum confirms the bond formation in the samples and decrease in ϵ' and with increase loss tangent ($\tan\delta$) in frequency for these samples suggests the dielectric dispersion behavior. The dispersion is more

pronounced in Sr-rich compositions. The frequency dependence of ac conductivity show that ac resistance follows universal power law.

Acknowledgement:

One of the authors Dr. Vijaya Puri is gratefully acknowledged to UGC for the Award of Research Scientist 'C'.

REFERENCES

- [1] M.O. Ramírez; D. Jaque, L.E. Bausá, J. García Solé, A.A. Kaminskii, *Phys. Rev. Lett.* 95 ,267401, (2005)
- [2] S.N. Murty, K.V.R. Murty, K.C. Mouli, A. Bhanumathi, S.B.Raju, G. Padmavathi, K.L. Murty, *Ferroelectrics* 158 ,325, (1994)
- [3] Y. Xu, *Ferroelectric Materials and their Applications*, Elsevier Science Publishers, NewYork, (1991)
- [4] M.-H. Li, X.-W. Xu, D. Qiu, T.-Ch. Chong, H. Kumagai, M. Hirano, *J. Crystal Growth* 211, 225 (2000)
- [5] Goulkov M, Imlau M, Granzow T and Woike J. *Appl.Phys.* 94 ,4763, (2003)
- [6] Granzow T, Woike Th, W'ohlecke M, Imlau M and Kleemann W *Phys. Rev. Lett.* 89 ,127601 , (2002)
- [7] Ram ´irez M O, Romero J J, Molina P and Baus´a L E ,*Appl. Phys. B* 81 827,(2005)
- [8] S.G. Lu, C.L. Mak, and K.H. Wong, *J. Am. Ceram. Soc.*, 84, 79, (2001)
- [9] T. Fang, N.Wu, and F. Shiau, *J. Mat. Sc. Lett.*, 13, 1746, (1994)
- [10] Myoung-SupKim, Joon-Hyung Lee, Jeong-Joo Kim,, Hee Young Lee, Sang-Hee Cho *Journal of the European Ceramic Society* 22 ,2107,(2002)
- [11] Yong-Quan Qu, Ai-Dong Li, Qi-Yue Shao, Yue-Feng Tang, Di Wu ,C. L. Mak, K. H. Wong and Nai-Ben Ming *Materials Research Bulletin* 37, 503, (2002)
- [12]Qing-Wei Huang a, Pei-Ling Wang, Yi-Bing Cheng ,Dong-Sheng Yan. *Materials Letters* 56 , 915, (2002)
- [13] S S Shinde, P S Shinde, C H Bhosale and K Y Rajpure *J. Phys. D: Appl. Phys.* 41 105, (2008)
- [14]A. Speghini, M. Bettinelli, U. Caldi ño, M.O. Ramírez, D. Jaque, L.E. Bausá, J. GarcíaSolé, *J. Phys. D: Appl. Phys.* 39,4930, (2006)
- [15]Jamieson P B, Abrahams S C and Bernstein J L *J. Chem.Phys.* 48, 5048, (1968)
- [16]D. Kasprowicz , A. Lapinski , T. Runka , A. Speghini , M. Bettinelli *Journal of Alloys and Compounds* 478 ,30, (2009)
- [17]George M, Nair S S, Malini K A, Joy P A and Antharaman M R *J. Phys. D: Appl. Phys.* 40 ,1593, (2007)
- [18]E Buixaderas, M Savinov, M Kempa, S Veljko, S Kamba, J Petzelt,R Pankrath and S Kapphan, *J. Phys.: Condens. Matter* 17 ,653, (2005)
- [19]Shaikh A M, Bellard S S and Chougule B K *J. Magn. Magn. Mater.* 195, 384, (1999)
- [20]C. Elissalde and J. Ravez *J. Mater. Chem.*, 10, 681, (2000)
- [21]P. A. Jadhav, M. B. Shelar and B. K. Chougule, *Archives of Physics Research I*, 92, (2010):
- [22]P. Dasaria , K. Sambasiva Rao , P. Murali Krishna and G. Gopala Krishna, *Acta Physica Polonica A* ,1,19 (2011)